Title: Bacterial Volatile Organic Compound Specialists in the Phycosphere

Short title: Bacterial VOC specialists in the phycosphere

Authors: Vaishnavi G. Padaki[1], Xavier Mayali[2], Peter K. Weber[2], Stephen J. Giovannoni[1], Kaylene Abraham[1], Kerry Jacobs[1], Lindsay Collart[1], Kimberly H. Halsey[1*]

Author Affiliations:

[1] Department of Microbiology, Oregon State University

[2] Lawrence Livermore National Laboratory, Livermore, CA 94550 USA

[*]Corresponding author

Abstract:

Labile dissolved organic carbon (LDOC) in the oceans accounts for ~¼ of marine primary production and turns over with a half-life of seconds to days, fueling one of the largest engines of microbial heterotrophic production on the planet. Volatile organic compounds (VOCs) are poorly constrained components of LDOC. Here, we detected 78 *m*/*z* signals, corresponding to unique VOCs, including petroleum hydrocarbons, totaling 18.5 nM in the culture medium of a model diatom. In five cocultures with bacteria adapted to grow with this diatom, 1 to 66 VOCs were depleted. Two of the most active VOC consumers, *Marinobacter* and *Roseibium,* contained more genes encoding VOC oxidation proteins, and attached to the diatom, suggesting VOC specialism. With NanoSIMS and stable isotope labeling, we confirmed that *Marinobacter* incorporated carbon from benzene, one of the depleted VOCs detected in the co-culture. Diatom gross carbon production increased by up to 29% in the presence of VOC consumers, indicating that VOC consumption by heterotrophic bacteria in the phycosphere – a region of rapid organic carbon oxidation that surrounds phytoplankton cells – could impact global rates of gross primary production.

Keywords:

Phycosphere, Volatile organic compounds, Algal-bacterial interactions, Phytoplankton photosynthesis, Hydrocarbon metabolism

Introduction:

The majority of algal primary production in the world oceans is labile dissolved organic carbon (LDOC), which is readily catabolized by heterotrophic bacteria [1]. Volatile organic

31 compounds (VOCs) are an important subset of the LDOC produced by phytoplankton [2], but
32 VOCs are often overlooked in metabolomic studies because most are not captured by common
33 methods of analysis such as solid phase extraction and liquid chromatography. VOCs are
34 involved in complex allelochemical processes in the marine ecosystem [3]. Some VOCs defend
35 against algal predation (reviewed in Saha and Fink 2022) [3], but dimethylsulfide (DMS)
36 stimulates grazer activity [4]. VOCs can inhibit algal competitors [5] and signal within-population
37 stress [6]. VOC emissions from the ocean into the atmosphere contribute to secondary aerosols and
38 alter the oxidative capability of the atmosphere. These climate impacts make understanding the
39 biological processes that control VOC accumulation in the surface oceans of utmost importance.

40 Some VOCs, such as isoprene and DMS, are produced by phytoplankton in response to
41 stress [4,7,8], while others (e.g., acetaldehyde and methyl iodide) are intermediate chemicals in
42 metabolic pathways [9,10] that can diffuse across cell membranes due to their low molecular
43 weights and hydrophobicity. These diffusive properties may allow VOCs to escape biochemical
44 transformation and cross the algal cell membrane. Other VOCs, including aromatic hydrocarbons
45 such as benzene, toluene, and ethylbenzene/xylene (collectively known as BTEX), are produced
46 by phytoplankton via the shikimate and non-mevalonate pathways. [11,12]

47 The multifaceted effects of VOCs suggest they have a role in structuring the microbial
48 community. Research on VOC transfer between algae and bacteria shows that VOCs, including
49 DMS, released by algae can be growth substrates for marine bacteria[13,14]. For example, a wide
50 range of VOCs were detected during the growth of the diatom *Thalassiosira pseudonana*, and a
51 subset of those supported the growth of *Pelagibacter ubique* HTCC1062, a member of the
52 ubiquitous SAR11 bacterioplankton [10,15]. These publications suggested that VOCs were "public
53 goods" released by the diatom constitutively and available to any organism able to metabolize

them. *P. ubique* metabolized isoprene, acetone, acetaldehyde, DMS, and cyclohexanol, which include some of the most well-studied VOCs for their roles in air-sea exchange and atmospheric chemistry [15]. BTEX are produced by some algae [11], and are growth substrates for a wide variety of bacteria isolated from oilfields [16,17], soils [18], groundwater [19], and wastewater [20]. Less is known about BTEX consumption by marine bacteria, which is likely an important sink that limits BTEX emissions into the atmosphere [2]. Genes encoding proteins that oxidize some VOCs (e.g., methanol, DMS, acetone, acetaldehyde) in bacteria have been elucidated [14]. In the ocean, the widespread expression of some of the genes involved, such as acetone/cyclohexanone monooxygenase, suggests marine bacteria have an important role in mediating VOC air-sea emissions [10].

The phycosphere, the layer of water immediately surrounding a microalgal cell, is the site of complex interactions between phytoplankton and bacterioplankton, which influence carbon and nutrient cycling in marine ecosystems [21–23]. Microbial activities in the phycosphere are believed to be distinct from processes occurring in bulk water, a result of bacterial taxa with specialized adaptations populating the region of concentrated chemicals surrounding phytoplankton [24,25]. Direct chemical transfer from phytoplankton to bacterioplankton should be enhanced by their occupation of the narrow zone of the phycosphere, which allows access to metabolites before they diffuse into the bulk seawater [22,26]. The ecology of the phycosphere is similar to its terrestrial analog, the rhizosphere: phylogenetically related bacterial taxa are found across both systems [27], chemotaxis plays a central role in accessing the narrow zone of high chemical concentration [28,29], and the chemicals transferred from the primary and secondary producers are functionally similar [22]. For example, primary metabolites, such as sugars, amino acids, and vitamins, as well as metabolite precursors, such as organosulfur compounds

77 (dimethylsulfide (DMS) and dimethylsulfoniopropionate) [30,31], are used as bacterial growth
78 substrates in both the phycosphere and rhizosphere [32,33].

79 The bacterial community in the phycosphere of marine microalgae may be uniquely
80 adapted to VOC metabolism, as is the case for methylotrophs in the phyllosphere [34]. The
81 phycosphere of a modest-sized (~20 μm) diatom extends about 50 – 2000 μm away from the cell
82 [22]. In this region, chemicals released by algae are modeled to be ≥50% higher in concentration
83 than in bulk seawater [22], where VOC concentrations are in the fM to nM range. VOC
84 concentration in the phycosphere is partly controlled by the rate of diffusion from the algal
85 source. The rate of diffusion decreases with increased molecular size and decreased
86 hydrophobicity and likely increases with phytoplankton growth rate and bacterial VOC uptake.
87 Some bacteria occupy the phycosphere through chemotaxis or physical attachment to algal cells
88 [35,36]. Chemotactic bacteria experience transient exposures to a dynamic organic chemical cocktail
89 in the phycosphere [32], where the composition depends on the algal producer [21,37], environment
90 [38,39], and antagonistic and mutualistic interactions [32,40,41], requiring bacterial consumers to
91 efficiently shift physiologies to match resource availability. Strategies bacteria use to navigate
92 carbon acquisition as they traverse phycosphere boundaries are not known but may depend on
93 pool sizes and the diversity of regulatory behavior systems for the uptake and metabolism of
94 various substrates [42]. Bacteria that can adhere to algae would, in principle, optimize diffusion-
95 mediated VOC uptake by positioning themselves most closely to the algal source.

96 Diatoms can develop massive spring blooms and are responsible for about half of
97 photosynthesis in the oceans [43]. *Phaeodactylum tricornutum* is a model diatom whose
98 photophysiology has been extensively studied for ecological and bioenergy purposes. Here, we
99 investigated VOC transfer from the model diatom, *Phaeodactylum tricornutum,* to phycosphere

100 bacteria previously isolated from an outdoor *P. tricornutum* production pond. The bacteria varied
101 in taxonomy, DOC uptake, and attachment to the diatom, and are representive of families
102 (*Rhodobacteriacea*, *Alteromonadaceae*) ubiquitously found in biofuel production ponds as well
103 as the oceans [32,44,45]. Results show VOC transfer from *P. tricornutum* to its phycosphere bacteria
104 fuels primary and secondary production. Extrapolated to larger scales, our findings support the
105 perspective that phycosphere bacteria are a sink for up to 29% of gross carbon production
106 through VOC transfer, and they play a critical role in limiting VOC accumulation in the surface
107 ocean.

108 **Materials and Methods**:

109 *Culture growth and P. tricornutum physiology:*

110 *Phaeodactylum tricornutum* strain CCMP 2561 was maintained axenically and in
111 separate co-cultures with *Roseibium* sp. 13C1, *Yoonia* sp. 4BL, *Marinobacter* sp. 3-2,
112 *Rhodophyticola* sp. 6CLA, and *Stappia* sp. ARW1T (herein "PT-bacteria genus name"). Cultures
113 were grown under 12h:12h light: dark cycles (60-70 µmol photons m^{-2} s^{-1}), at 19ºC in f/2+Si
114 medium (ASW) [46]. DAPI (NucBlue, Thermo Fischer) and fluorescence microscopy were used to
115 check *P. tricornutum* axenicity. Bacterial and diatom growth were determined in triplicate. Cell
116 densities were measured using a GUAVA flow cytometer (Millipore; Billerica, MA, USA) 1-2 h
117 into the light phase. VOCs, chlorophyll content (Chl*a*), and photosynthetic efficiency (F_v/F_m)
118 were measured 4-6 h into the light phase. Chl*a* was determined from filtering 2-5 ml of culture
119 (GF/F, Whatman, 25 mm), extracting in 5 ml 90% acetone, and storing at -20º C for 24 h. Chl*a*
120 was quantified by spectrophotometer (Shimadzu; Kyoto, Japan) [47]. F_v/F_m was measured by fast
121 repetition-rate fluorometer following 10 min dark acclimation [48]. Short-term carbon fixation rates

122 (approximating gross carbon production, GCP) were measured as in Moore et al. (2020)[15]. In
123 that work, uptake of VOCs by *P. ubique* HTCC1062 in coculture with *T. pseudonana* stimulated
124 GCP ~20% compared to the *T. pseudonana* monoculture. VOC uptake was confirmed as the
125 cause of the boost in GCP when GCP increased ~20% after a hydrocarbon trap was installed in
126 the *T. pseudonana* monoculture to simulate a highly efficient VOC "sink." In our experiment,
127 axenic *P. tricornutum* was grown in a closed system with culture headspace recirculating at 80
128 ml min^{-1} by peristaltic pump and either directed back into the culture medium or passed first
129 through a hydrocarbon trap (Marineland Black Diamond Activated Carbon) and then into the
130 medium. Headspace in *P. tricornutum*-bacteria cocultures was recirculated in the same manner
131 with no hydrocarbon trap. Flasks containing only ASW were recirculated for 24 h prior to
132 inoculation with the cultures to remove background VOCs. Samples for $^{14}CO_2$-uptake (10 ml)
133 were collected by syringe during the *P. tricornutum* exponential phase (2-4 x 10^5 cells ml^{-1}),
134 spiked with 2 μCi of ^{14}C-sodium bicarbonate and incubated 20 min in light or dark. All samples
135 were acidified and vented for 24 h prior to measurement by scintillation counter.
136
137 *VOC measurement by PTR-TOF/MS*

138 VOCs were measured in axenic *P. tricornutum* and cocultures by PTR-TOF/MS (PTR-
139 TOF1000, Ionicon, Austria), as in Moore et al. (2020)[15]. VOCs in ASW and HPLC-grade water
140 were measured alongside the samples as blank controls. Culture, ASW, or HPLC water (100 ml)
141 was transferred to a 0.2 L polycarbonate dynamic stripping chamber[49] and bubbled with
142 breathing-grade air passed first through a hydrocarbon trap and then through a glass frit in the
143 bottom of the chamber at 50 ml min^{-1} for 5 min to strip VOCs from the sample. Stripped VOCs
144 were directed into the PTR-TOF/MS for detection following soft ionization with H_3O^+. Mass

145 spectra (30-240 a.m.u.) were acquired every 5 s. Each peak in the spectra is a compound of its
146 molar mass + 1.008 (mass of H^+). Data from 0.5-5 min were analyzed for VOCs. PTR-TOF/MS
147 data were processed using PTR-viewer 3.4.3 (Ionicon Analytik). h5 files were mass-calibrated
148 using three chemicals known within all spectra (*m*/*z* 29.998, 203.943, and 330.848). First, *m*/*z*
149 signals were binned at 0.5 mass units bounded by 0.25 and 0.75 mass units. Examination of each
150 bin was done to detect multiple peaks within the same bin. A Gaussian-based approach was used
151 to determine the *m*/*z* of each individual peak. Known contaminants, internal standards, water
152 clusters, and fragments of identified parent compounds were removed from further analysis.[52]
153 Isomeric compounds are not discriminated by PTR-TOF/MS. When possible, *m*/*z* signals were
154 associated with a chemical formula and tentatively identified based on the PTR-Viewer 3.4.3,
155 Ionicon integrated "ChemSpider" database, the GLOVOCS compound assignment database [50],
156 and the literature. *m*/*z* signals were categorized into functional groups using the "ChemSpider"
157 database. *m*/*z* signals having isomers in different functional groups were categorized as "mixed."
158 Integrated peak signals were normalized to H_3O concentration and detected analyte
159 concentrations (ppbv) calculated without calibration using the simple-reaction-kinetics approach
160 with 30% accuracy for *E/N* values >100Td [51] (*E/N* for this study = 126Td).

161 Analyte concentrations were converted from ppbv to molarity using the formula

162 $$C_t = \frac{[C_c - C_b] \cdot Q \cdot p \cdot t}{V \cdot R \cdot T}$$

163 where C_t is the *m*/*z* molar concentration in the *P. tricornutum* monoculture or PT-bacteria
164 coculture, C_c *is* the mixing ratio of the *m*/*z* in the headspace of the bubbled culture, C_b is the
165 mixing ratio of the *m*/*z* in the headspace of bubbled ASW, Q is the bubbling rate (0.3 L h^{-1}), p is

166 1 atm, *t* is the duration of the collected data (4.5 min), *V* is the volume of the culture (0.1 L), *R* is
167 the gas constant (0.0821 L atm K^{-1} mol^{-1}), and *T* is temperature (K).

168 *Benzene uptake and nanoSIMS analyses*:

169 Dose experiments were performed to evaluate the growth responses of *Marinobacter, Roseibium,*
170 *Rhodophyticola, and Stappia* to benzene addition (Supplementary Fig. S1). A saturated benzene
171 solution was prepared in ASW and added to 0.15 L ASW or *P. tricornutum*-spent media ('PT-
172 spent' prepared from 0.2 µm filtered spent media collected from axenic *P. tricornutum* grown to
173 2-4 x 10^5 cells ml^{-1} and diluted in 1:10 with ASW) in Teflon sealed 0.16 L crimp bottles to
174 obtain final concentrations ranging from 0 to 180 µM prior to bacterial inoculation. Cultures,
175 including no bacteria controls, were incubated at 19ºC in the dark and cell density measured
176 daily by withdrawing 0.5 ml by syringe.

177 ^{13}C-benzene uptake was evaluated using nanoSIMS in six different treatments grown in Teflon-
178 sealed bottles (*Marinobacter*) or airtight Nalgene bottles (*Rhodophyticola*). 50 nM 98% ^{15}N
179 leucine (Cambridge Isotopes, MA, USA) was added to all treatments as an independent measure
180 of cell activity. Sample preparation for nanoSIMS and description of isotopic measurements are
181 in Supplementary Fig. S2.

182 *SEM imaging*

183 Samples (5 ml) of *Marinobacter, Roseibium,* and *Rhodophyticola* cocultured with *P. tricornutum*
184 were collected in mid-exponential phase, treated with 1.25 ml of 2X 5% glutaraldehyde + 2%
185 paraformaldehyde (PFA) in 0.1 M sodium cocadylate buffer (NaCB), incubated for 24 h, filtered
186 on a 0.2 µm polycarbonate filter, and washed three times with NaCB + Milli-Q water. The

187 filtered cells were subjected to critical point drying and then vacuum-dried and gold-coated.
188 Imaging was done using a detector with a 5.1 mm working distance, 1.8 kV voltage, and 20-30
189 µm aperture diameter at the Electron Microscope facility, LPSC, Oregon State University. The
190 number of bacteria adhered to *P. tricornutum* in coculture was estimated from 50 diatom cells
191 (Supplementary Table S1).

192 *Bacterial genes encoding hydrocarbon metabolism*

193 Whole genome sequences of each bacteria were acquired from NCBI (GB accession numbers:
194 *Marinobacter*: PRJNA500125; *Rhodophyticola*: PRJNA441682; *Yoonia*: PRJNA441685;
195 *Stappia*: PRJNA441689; *Roseibium*: PRJNA441686). Geneious Prime v2023.2.1 and Hidden
196 Markov Models were used to search genomes for genes encoding proteins initiating hydrocarbon
197 oxidation (i.e., *alkB*, Pfam(PF00487); *almA*, Pfam(PF00743); *rhdA*, Pfam(PF00848); *acmA*,
198 Pfam(PF00743); *aldH*, Pfam(PF00171) (Supplementary Table S2) [52]. Each hit for *alkB* and *rhdA*
199 was manually curated using Geneious Prime v2023.2.1. Each hit with bit-score of ≥50 and e-
200 value > 0.001 [53] was aligned using MUSCLE protein alignment [54] in Geneious prime v2023.2.1.

201 *Statistics*

202 Statistical analyses and figure construction were done in R studio v.4.1.1, with ggplot2 and
203 Complex heatmap packages [55,56]. Paired student t-tests ($p \leq 0.05$) were used to identify *m*/*z*
204 signals that were detected at different concentrations between treatments. The Benjamini-
205 Hochberg procedure was used to control the false detection rate with *m*/*z* signals with Q-values >
206 0.1 removed from further analysis. Principle component analysis and Permutational Multivariate
207 Analysis of Variance (PERMANOVA) were used to evaluate VOC accumulation and depletion
208 patterns between cultures.

209 **Results**:

210 *Phaeodactylum tricornutum produced a wide range of VOCs in culture*

211 During exponential growth of *P. tricornutum*, 78 *m/z* signals were detected by proton
212 transfer reaction mass spectrometry (PTR-MS) at concentrations higher than the media control
213 [multiple t-test corrected p-value at 0.1 (FDR_{B-H}<0.1, n = 6)]. VOCs accumulated in the culture
214 to a total of 85.1 fmol $cell^{-1}$, or 18.5 nM, and represented eight known chemical functional
215 groups (Fig. 1). Hydrocarbons represented about 60% of the VOCs produced in the exponential
216 phase (54.2 fmol $cell^{-1}$; Supplementary Table S3) and included BTEX compounds (*m/z* 79.11,
217 *m/z* 93.07, and *m/z* 107.08), respectively, previously reported in *P. tricornutum* [11], and $C_{11}H_{16}$
218 (*m/z* 149.13). Alcohols were the second most abundantly produced group of VOCs, contributing
219 up to 11% of the total VOC pool (10.2 fmol $cell^{-1}$). Methanol (*m/z* 33.03) and, likely, ethanol
220 (*m/z* 47.04) made up the vast majority of the accumulated alcohols. Consistent with reports that
221 *P. tricornutum* is a halocarbon producer [57,58], *m/z* 124.96, corresponding to bromoethanol, was
222 detected in the exponential phase. The well-studied VOCs acetone (*m/z* 59.05), acetaldehyde
223 (*m/z* 45.03), and DMS (*m/z* 63.03) were also detected in the exponential phase.

224 After *P. tricornutum* entered the stationary growth phase, 58 *m/z* signals were detected in
225 concentrations higher than the media control (FDR_{B-H}<0.1, n = 6) and accumulated to 9.01 fmol
226 $cell^{-1}$, or 0.96 fM (Fig. 1), which was only about 10% of the VOC accumulation during the
227 exponential phase (Fig. 1, Supplementary Table S3). VOCs detected in both phases of growth
228 were consistently lower in concentration in the stationary phase. Slower VOC production in
229 response to cessation of growth, and loss of VOCs from the vented growth flasks, are the most
230 likely explanations for the concentration differences between growth phases. Hydrocarbons still

231 represented most of the VOCs (84%) but their production was only 7.59 fmol cell^{-1}. Sixteen of
232 the 58 *m*/*z* signals were unique to the stationary phase, but many of these had unknown identities.

233 The most abundant VOC in both exponential and stationary phases was *m*/*z* 149.13,
234 accumulating to 32.5 and 4.9 fmol cell^{-1} in each growth phase, respectively. This *m*/*z* signal
235 corresponds to the unprotonated formula $C_{11}H_{16}$, a hydrocarbon with isomers including
236 dictyopterene D', which was previously detected in brown algae[59,60]. *m*/*z* 149.13 also
237 corresponds to the aromatic hydrocarbons, neopentyl-benzene, 4-tert-butyl-toluene, and 1-ethyl-
238 2-propylbenzene, which have been identified in plant leaves [61]. Forty-two *m*/*z* signals, including
239 BTEX, were detected in both exponential and stationary phases (Fig. 1).

240 *VOCs were depleted in P. tricornutum-bacteria cocultures*

241 Five *P. tricornutum*-bacteria cocultures were grown to identify VOCs produced by the
242 diatom that decreased in concentration in the presence of a bacterium, which would suggest
243 those VOCs were consumed by the bacterium. Alternatively, lower VOC concentrations in a
244 coculture could indicate VOC production was inhibited in the presence of the bacterium. The
245 five *P. tricornutum*-bacteria cocultures (herein "PT-bacteria genus name") each showed distinct
246 VOC depletion patterns during exponential growth when compared to axenic *P. tricornutum*
247 (Fig. 2a, Supplementary Fig. S3, PERMANOVA, p-value = 0.03, n = 6). Of the 78 *m*/*z* signals
248 produced by *P. tricornutum* in exponential phase, 31 to 59 were significantly depleted in four of
249 the five cocultures ($FDR_{B\text{-}H}<0.1$, n = 6) (Fig. 2a). VOCs were most strongly depleted in PT-
250 *Marinobacter* (7.09 fmol cell^{-1}), followed by PT-*Stappia* (6.51 fmol cell^{-1}), PT-*Roseibium* (5.52
251 fmol cell^{-1}) and PT-*Rhodophyticola* (4.54 fmol cell^{-1}), where VOC depletion was normalized to
252 the concentration of bacterial cells in the coculture (Fig. 2a, Fig. 4, Supplementary Table S4).

253 About half the number of *m*/*z* signals were depleted in the PT-*Roseibium* compared to PT-
254 *Marinobacter*. Some *Marinobacter* and *Roseibium* cells were observed to be attached to *P.*
255 *tricornutum* (Fig. 3) [44], thus the cell-normalized VOC depletion data in PT-*Marinobacter* and
256 PT-*Roseibium* are based on estimates of bacteria cell densities using flow cytometry for the free-
257 living and scanning electron microscopy for the attached bacteria (see Methods, Supplementary
258 Table S1). In PT-*Yoonia*, only one *m*/*z* signal, 45.03, corresponding to acetaldehyde, was
259 significantly depleted (0.5 fmol $cell^{-1}$ (Fig. 2a, Supplementary Table S4). There were 14 *m*/*z*
260 signals that did not show significant depletion in any of the five PT-bacteria cocultures. A lack of
261 depletion could mean that the bacteria could not incorporate or metabolize those VOCs, or those
262 VOCs were maintained at a steady state concentration by equal rates of production and
263 consumption in the coculture. Of those, 5 *m*/*z* signals belonged to the nitrogen-containing
264 category of VOCs (Supplementary Table S5). Furthermore, neither methanol nor acetone were
265 depleted in any of the five cocultures.

266 Hydrocarbons were the most highly depleted group of VOCs in all PT-bacteria cocultures
267 except PT-*Yoonia*. Depending on the bacterium present, 10-17 of the depleted *m*/*z* signals were
268 classified as hydrocarbons and made up to 70% of the total VOC pool depleted in the cocultures.
269 PT-*Marinobacter* depleted the most hydrocarbons (5.95 fmol $cell^{-1}$), followed by PT-*Stappia*
270 (5.44 fmol $cell^{-1}$), PT-*Roseibium* (4.48 fmol $cell^{-1}$) and PT-*Rhodophyticola* (3.94 fmol $cell^{-1}$)
271 (Fig. 2a). Monoaromatic hydrocarbons, including BTEX, $C_{11}H_{16}$, and *m*/*z* 103.05 (likely
272 corresponding to phenylacetylene), were the most strongly depleted hydrocarbons in the PT-
273 bacteria cocultures (Fig. 2a).

274 In stationary phase, the range of depleted VOCs in the PT-bacteria cocultures was lower,
275 from 0.64-4.97 fmol $cell^{-1}$ (average 2.96 ± 0.66 fmol $cell^{-1}$). The depletion patterns between PT-

276 bacteria cocultures in stationary phase were not distinct from one another (Fig. 2b,
277 Supplementary Fig. S3, PERMANOVA p-value = 0.22, n = 6). In total, 24 to 55 *m*/*z* signals were
278 depleted in the PT-bacteria cocultures ($FDR_{B\text{-}H}$<0.1, n = 6). The number of *m*/*z* signals depleted
279 in PT-*Yoonia* expanded from 1 in the exponential phase to 24 in the stationary phase, but the
280 amounts of the individual VOCs depleted were low (Fig. 2b, Supplementary Tables S4 and S7).
281 In stationary phase, 8-14 *m*/*z* signals depleted in PT-bacteria cocultures were classified as
282 hydrocarbons, and these VOCs were the majority of the depleted VOC pools (80-92%). VOCs
283 classified as carboxylic acids were the second-most depleted group, followed by ketones (Fig. 2a
284 and b). Except for hydrocarbons, the magnitude of VOC depletion in PT-bacteria cocultures did
285 not mirror VOC abundances in axenic *P. tricornutum* in either growth phase.

286 *Bacterial VOC uptake comprised up to 29% of gross carbon production*

287 *P. tricornutum* growth rates, chlorophyll content, and photosynthetic efficiencies were
288 unaffected by the presence of any of the bacterial species in the PT-bacteria cocultures
289 (Supplementary Table S6). To assess the impact of bacterial VOC uptake on *P. tricornutum*
290 primary production, short-term $^{14}CO_2$-uptake rates, approximating gross carbon production
291 (GCP) were measured. GCP in PT-bacterial co-cultures were higher in PT-*Marinobacter,* PT-
292 *Stappia,* and PT-*Rhodophyticola* than in axenic *P. tricornutum* (Fig. 4). To confirm that VOC
293 uptake, rather than non-volatile DOC uptake, increased GCP in the cocultures, a hydrocarbon
294 trap was installed that stripped VOCs from the axenic *P. tricornutum* culture, simulating a highly
295 efficient bacterial VOC sink. This treatment caused GCP to increase by 24.9% compared to
296 axenic *P. tricornutum* with no trap (Fig. 4; p = 0.025, n = 6). GCP in PT-*Marinobacter,* PT-
297 *Rhodophyticola,* and PT-*Stappia* were similar to axenic *P. tricornutum* with the hydrocarbon trap
298 and 20.1% to 29.3% higher than in axenic *P. tricornutum* (p-values < 0.05, t-tests, n=3). These

299 differences in GCP corresponded to 0.05 to 0.12 nmol C $cell^{-1}$ h^{-1} transferred from *P.*
300 *tricornutum* to the bacteria in the form of VOCs (Fig. 4). Consistent with the minimal amount of
301 VOC depleted in PT-*Yoonia*, there was no difference in GCP between PT-*Yoonia* and axenic *P.*
302 *tricornutum* (p-value = 0.23, t-test, n=3). GCP was not stimulated in PT-*Roseibium* until
303 *Roseibium* entered the second exponential growth phase in its diauxic growth pattern (Fig. 2;
304 note lag between days 2 and 4). This result suggests that *Roseibium* shifted carbon uptake from
305 primarily LDOC early in culture growth to primarily VOCs later in culture growth. VOC
306 depletion in the PT-bacteria cocultures appears to be low compared to the rate of VOC uptake
307 determined by differences in GCP. However, VOC depletion data likely significantly
308 underestimate bacterial VOC uptake because VOC concentrations in the cocultures reflect only
309 slight differences in steady state rates of VOC production and consumption.

310 *VOC depletion correlates with genome content for hydrocarbon metabolism*

311 Of the five bacteria tested*, Marinobacter* and *Roseibium* genomes harbor the largest
312 number of genes encoding hydrocarbon oxidation proteins. For example, genes identified in
313 *Marinobacter* and *Roseibium* included *rhdA,* encoding ring hydroxylating dehydrogenase, *almA*,
314 encoding flavin-binding monooxygenase involved in long-chain alkane degradation, and *alkB,*
315 encoding alkane monooxygenase. RhdA is in a superclass of nonheme iron enzymes that convert
316 aromatic hydrocarbons to dihydrodiols in the presence of dioxygen and NADH [62]. The broad
317 substrate range for RhdA includes benzene, and the benzene-alkyl substituted hydrocarbons
318 toluene, ethylbenzene, and xylene, consistent with BTEX depletion profiles in *Marinobacter* and
319 *Roseibium*. Benzene dioxygenases are a subclass of RhdA that oxidize benzene and toluene to
320 their corresponding dihydrodiols. We manually curated the *rhdA* hits for *bnzA*, encoding the α-
321 subunit of the benzene 1,2 dioxygenase hydroxylase, based on conservation of the active site

322 motif Cys-X_1-His-15-to-17 aa-Cys-X_2-His (where X is any amino acid) [63]. The gene, *bnzA,* was
323 identified in *Marinobacter*, *Rhodophyticola*, and *Roseibium* (Fig. 2d). The gene, *bnzB,* encoding
324 the β-subunit of benzene 1,2 dioxygenase hydroxylase, was also identified in *Marinobacter* (Fig.
325 2d). The presence of both α and β-subunits increases hydroxylation activity compared to the
326 activity of either of the subunits alone [64]. Genes encoding hydrocarbon oxidation in *Stappia* were
327 not identified. Acetone/cyclohexanone monooxygenase, encoded by *acmA* was identified in
328 *Marinobacter, Roseibium, and Stappia*. The broad substrate range of acetone/cyclohexanone
329 monooxygenase [65,66] may include cyclic ketones, such as valerophenone (*m*/*z* 163.11) and E-
330 jasmone (*m*/*z* 165.13), corresponding to *m*/*z* signals that were depleted in PT-*Marinobacter*, PT-
331 *Roseibium*, and PT-*Stappia*. One or two copies of *aor,* encoding aldehyde dehydrogenase, were
332 identified in each of the five bacteria, consistent with acetaldehyde (*m*/*z* 45.03) depletion in the
333 five cocultures (Fig. 2).

334 *Marinobacter* and *Rhodophyticola exhibited distinct benzene metabolism*

335 We selected benzene as a representative hydrocarbon to directly test incorporation into
336 biomass by *Marinobacter* and *Rhodophyticola*. These bacteria differed in the amounts of
337 benzene depleted in the PT-bacteria cocultures, in their molecular capacities for hydrocarbon
338 metabolism and chemotaxis, in their attachment physiologies (Fig. 2, 3) [44], and could be grown
339 without *P. tricornutum* in media prepared from filtrate collected from *P. tricornutum* in
340 exponential growth ('PTspent'; see methods). Benzene supported growth of *Marinobacter*, but
341 not *Rhodophyticola,* in ASW, and both bacteria grew to higher cell densities in PTspent with
342 added benzene vs. no added benzene (Supplementary Fig. S1; Fig. 5). Benzene uptake and
343 subsequent incorporation into biomass by *Marinobacter* and *Rhodophyticola* were quantified
344 using nanoSIMS. We incubated each bacterium with and without ^{13}C benzene (60 μM in

345 *Marinobacter* cultures, 36 µM in *Rhodophyticola* cultures) and ^{15}N leucine (50 nM), in f/2+Si
346 artificial seawater medium (ASW), PTspent medium, and in coculture with *P. tricornutum*.
347 *Marinobacter* cell densities were higher in ASW with benzene added as the sole source of
348 carbon compared to ASW with no benzene added (Fig. 5a p-value <0.05, n = 3). Associated C_{net}
349 values of incorporation, measuring the fraction of a cell's C originating from benzene, increased
350 over the incubation period, reaching 0.03 to 0.15 (average 0.065, or 6.5%) on day 7 (Fig. 5b).
351 *Marinobacter* reached higher cell densities in PTspent with added benzene compared to PTspent
352 with no benzene (Fig. 5a p-value <0.05, n = 3). Consistent with benzene-stimulated growth in
353 PTspent, *Marinobacter* C_{net} values in that treatment ranged from 0.02 to 0.17, averaging 0.07 on
354 day 4. *Marinobacter* cell densities were unaffected by benzene addition to PT-*Marinobacter*.
355 Interestingly, *Marinobacter* did not incorporate ^{13}C benzene in the presence of live *P.*
356 *tricornutum* cells. *Marinobacter* C_{net} values in the coculture averaged zero across the 10-day
357 incubation, even in the presence of 60 µM externally-supplied benzene (Fig. 5e). N_{net} values
358 from leucine in all *Marinobacter* treatments, including the coculture, were low, but higher than
359 killed cell controls (t-tests, p-values <0.01, Supplementary Fig. S2), confirming bacterial
360 activity.

361 Despite significantly higher *Rhodophyticola* cell densities in PTspent with 36 µM
362 benzene added compared to the no benzene-added control (Fig. 5c), ^{13}C-benzene addition to
363 PTspent resulted in low C_{net} values, and only 2% of the population showed enrichment in ^{13}C
364 benzene on day 6 (Fig. 5d). *Rhodophyticola* may take up and oxidize benzene for energy rather
365 than biomass generation. No significant difference was observed in *Rhodophyticola* cell densities
366 grown in the PT coculture with or without added ^{13}C-benzene. Similar to *Marinobacter*, C_{net}
367 values in *Rhodophyticola* grown in the PT coculture were very low. *Rhodophyticola* showed ^{15}N

368 enrichment from leucine in both PTspent and PT-*Rhodophyticola* treatments (Supplementary
369 Fig. S2).

370

371 **Discussion**:

372 Phycospheres are recognized as energy-rich regions of heterotrophic activity where
373 microbes adapted to this niche benefit from proximity to high concentrations of the organic
374 resources produced by phytoplankton cells. VOCs are diffusible molecules that easily traverse
375 cell membranes and, due to the introduction of new measurement technologies, are increasingly
376 recognized as complex and important products of phytoplankton metabolism. Here, we show that
377 the phycosphere concept applies to VOCs and that they appear to be an important component of
378 photosynthetic carbon transfer to heterotrophic microbial populations in the region immediately
379 surrounding phytoplankton cells. We also show that some phycosphere bacteria have traits that
380 can be interpreted as evidence of VOC specialism, enabling them to access these chemicals
381 whose concentrations are expected to decrease with distance from their source.

382 VOCs were primarily produced during active *P. tricornutum* growth, when over a quarter
383 of gross carbon production (GCP) was emitted from *P. tricornutum* as VOCs captured in a
384 hydrocarbon trap. Hydrocarbons represented 64% of the total VOCs produced, with BTEX
385 accounting for 13% of the emitted VOC pool, accumulating to 11.8 nM in the diatom culture.
386 BTEX production by phytoplankton has been proposed to be of sufficient magnitude to influence
387 atmospheric chemistry [11], unless bacterial VOC consumption prevents BTEX accumulation in
388 the surface ocean [2]. The VOC concentrations we measured could be underestimates of VOC
389 production because the cultures were grown in vented flasks. Furthermore, in the absence of

390 bacterial sinks, internal VOC concentrations in axenic *P. tricornutum* cells may reach equilibria
391 with the surrounding medium limiting ongoing VOC accumulation in cultures.

392 We measured concentrations of VOCs in diatom-bacteria cocultures relative to the
393 diatom grown alone to investigate the potential for VOC uptake by bacteria. In the case of
394 benzene, isotopic labeling confirmed that *Marinobacter* used benzene for biomass generation,
395 but for other VOCs, we cannot eliminate the possibility that VOC depletion in coculture was
396 caused by bacterial inhibition of VOC production by *P. tricornutum*. *P. tricornutum* GCP was
397 stimulated in cocultures where depletion of a wide range of VOCs was also observed. Some
398 marine bacteria are known to metabolize VOCs, including BTEX [15,67], and we showed that the
399 bacteria that caused VOC depletion also have genes encoding enzymes that oxidize some of the
400 depleted compounds. For other depleted compounds, genetic loci associated with bacterial
401 metabolism are unknown.

402 The data we report here indicate a range of bacterial VOC specialism (Table 1). Four of
403 the five bacterial strains harbor multiple genes that encode hydrocarbon oxidation enzymes with
404 broad substrate ranges. *Marinobacter* and *Roseibium,* which consumed large amounts of
405 hydrocarbons, had the most genes encoding for hydrocarbon oxidation. *Marinobacter* and
406 *Roseibium* had few genes encoding complex polysaccharide metabolism, and in previous
407 research, incorporated low amounts of macromolecular DOC into biomass [44]. In our
408 experiments, *Rhodophyticola* and *Stappia,* which harbor fewer hydrocarbon oxidation genes,
409 depleted smaller amounts of individual hydrocarbons but a wide range. Mayali et al. reported
410 that *Stappia, Rhodophyticola,* and *Yoonia* used complex DOC in their 2023 study, in agreement
411 with their larger array of genes encoding oligosaccharide, starch, and cellulose degradation [44].

412 Thus, for this set of traits, among a set of five heterotrophic isolates from *P. tricornutum* ponds,
413 two strains appeared to be VOC specialists: they used more VOCs and less carbohydrate DOM,
414 and as discussed below, they were motile and attached to *P. tricornutum*. Two strains used lesser
415 amounts of VOCs, are active metabolizers of carbohydrate DOM, are not motile, and did not
416 attach; and one strain used carbohydrate DOM, only a single VOC, and attached.

417 We searched for evidence of phycosphere occupation to understand whether, in the
418 strains we studied, it was linked to VOC use. The VOC specialists, *Marinobacter* and *Roseibium,*
419 and one strain that did not use VOCs, *Yoonia*, attached to *P. tricornutum,* but the other strains
420 did not. *Marinobacter* attached to the diatom in a flat orientation, while *Roseibium* attached to *P.*
421 *tricornutum* using polar adhesion (Fig. 3). It has been reported that chemotaxis and motility are
422 key traits of hydrocarbon-degrading bacteria. Volatile aromatic hydrocarbons, including toluene
423 and benzene derivatives, have been shown in previous work to be effective bacterial
424 chemoattractants, even in the presence of complex organic matter, such as petroleum, crude oil,
425 and diesel [68–70]. *Marinobacter* and *Roseibium* have canonical *che* genes, which encode for
426 chemotaxis [44], but chemoattractant compounds have not been identified in these bacteria [28,71]
427 (Table 1).

428 One of the most interesting results in this study was the absence of ^{13}C-benzene cellular
429 incorporation in *Marinobacter* grown in coculture with *P. tricornutum,* despite strong ^{13}C-
430 benzene incorporation in *Marinobacter* grown in the absence of *P. tricornutum* (i.e., in PTspent
431 and ASW) and significant benzene depletion in PT-*Marinobacter* compared to the *P.*
432 *tricronutum* monoculture (Fig 5). The experiment was repeated, and the results were confirmed.
433 These results suggest that in coculture with *P. tricornutum, Marinobacter* incorporated ^{12}C-

434 benzene, and possibly other hydrocarbons, directly from the diatom and specifically did not
435 incorporate ^{13}C-benzene from the bulk medium. *Marinobacter* and *Roseibium* were sometimes
436 observed attached to *P. tricornutum.* Bacterial attachment or entry into the phycosphere [28] could
437 facilitate efficient VOC transfer directly from the diatom to the bacteria. In coculture, VOC
438 uptake from the diatom to *Marinobacter* may occur via their physical interaction in flat
439 orientation, enabling passive VOC diffusion across the diatom and bacterial membranes. In
440 addition, FadL outer membrane transporters for hydrophobic molecules can boost BTEX
441 metabolism in some Gram-negative hydrocarbon degraders [72], and the *Marinobacter* strain used
442 in this study encodes a FadL protein with 72% nucleotide identity to the well-characterized FadL
443 in *Escherichia coli*. In the presence of the diatom, *Marinobacter* may regulate FadL to optimize
444 use of a wide range of substrates obtained from *P. tricornutum*. However, FadL substrate
445 specificity and kinetics are not yet known, and FadL may become saturated, inhibiting BTEX
446 uptake (i.e., the added ^{13}C-benzene in our experiment). Bacteria also exhibit varying preferences
447 for BTEX substrates [69] and the benzenoid collection of hydrocarbons. Benzene may be of lower
448 value to *Marinobacter* compared to the full collection of VOC substrates from growing *P.*
449 *tricornutum,* or benzene may be oxidized to CO_2 in the coculture rather than being incorporated
450 into biomass as was observed in ASW and PTspent. Nevertheless, the contrasting ^{13}C labeling
451 results in *Marinobacter* suggest attachment dynamics in the *P. tricornutum* phycosphere have an
452 important role in VOC uptake.

453 In the model set of phytoplankton and associated bacteria we investigated, phycosphere
454 resources were exploited by bacteria employing varying strategies: VOC specialists
455 (*Marinobacter* and *Roseibium*) that were motile and attached, generalists capable of VOC and
456 macromolecular uptake (*Rhodophyticola* and *Stappia*), and macromolecular specialists (*Yoonia*).

457 We hypothesize that VOC specialists use chemotaxis to find and colonize the phycosphere,
458 where proximity to sources of low molecular weight, rapidly diffusing VOCs offers advantages
459 [28]. Unknown is the duration of attachment or how hydrocarbon uptake is differentially regulated
460 in the presence and absence of *P. tricornutum*. The free-living generalists, *Rhodophyticola* and
461 *Stappia*, used VOCs and carbohydrate DOC and have fewer genes encoding hydrocarbon
462 oxidation proteins.

463 Collectively, VOC use by phycosphere bacteria was surprisingly broad in the range of
464 compounds used and increased gross carbon production up to 29% in *P. tricornutum.* These
465 findings add support to previous reports of VOC uptake by bacteria and stimulation of carbon
466 fixation in phytoplankton cocultured with VOC oxidizers. Previous reports show that balanced
467 production and consumption maintain low VOC concentrations in the oceans and have
468 associated VOC consumption with specialized metabolism in abundant, streamlined, non-motile
469 cells [49,73–75]. On the contrary, in the set of bacteria we studied, some of the most active VOC
470 utilizers were motile and attached to the phytoplankton. Our results suggest that VOC flux from
471 algae can be intercepted by VOC specialists in the phycosphere, reducing ocean VOC
472 accumulation and air-sea transfer and stimulating phytoplankton carbon production to replenish
473 lost VOC resources. If this conceptual model is correct, then it is conceivable that the
474 mechanisms we described result in a global increase in ocean photosynthetic carbon production
475 and are an important conduit of direct transfer of GCP to bacteria that does not rely on the
476 influence of protistan grazing and virus predation.

477

478

Table 1: Traits of bacteria used in this study. Plus symbols indicate the relative use of carbohydrate and VOC metabolism in each bacterium.

Bacteria	Carbohydrate metabolism[a]	VOC metabolism[b]	Flagellar biosynthesis (*flhA*)[c]	Chemotaxis (*che* genes)[a]	Attachment to diatom[a,b]
Marinobacter	+	+++	1 copy	Yes	Yes
Roseibium	+	+++	2 copies	Yes	Yes
Rhodophyticola	+++	++	Not present	No	No
Stappia	+++	++	Not present	No	No
Yoonia	+++	+	Not present	Yes	Yes

[a]Summarized from Mayali et al. 2023
[b]Summarized from this study
[c]*flhA* in *Marinobacter* has 72.9% amino acid similarity (e-value 2.58e-158) to *flhA* from *Escherichia coli* (P76298) and *flhA* in *Roseibium* have 64.5% (e-value 5.84e-106) and 67.0% (e-value 4.18e-89) amino acid similarity to P76298..

Data availability

All data generated or analyzed during this study is included in this published article [and its supplementary information files].

Acknowledgments

We thank Christina Ramon for lab assistance and Nicholas Baetge, Michael Sieler, and Chih Ping Lee for assistance with data analysis. This research was supported by award ID OCE1948163 to K.H.H. and S.J.G. from the National Science Foundation, Biological Oceanography Program. This research was supported in part by a fellowship to S.J.G. by the Hanse-Wissenschaftskolleg- Institute for Advance Study (HWK). Work at LLNL was Supported by the US Department of Energy's (DOE) Genomic Science Program through the LLNL µBioSpheres Science Focus Area grant # SCW1039 and performed under the auspices of the DOE under contract DE-AC52-07NA27344.

Author contributions

K.H.H., X.M., and V.G.P. conceived of the study. V.G.P. conducted all experiments with assistance from K.A., K.J., and L.C. and wrote the first manuscript draft with K.H.H. NanoSIMS was conducted by X.M. and P.K.W. Data analysis was done by V.G.P. All authors contributed to the final version of the manuscript.

Ethics declarations

The authors declare no competing interests.

References:

1. Carlson, C. A., Liu, S., Stephens, B. M. & English, C. J. DOM production, removal, and transformation processes in marine systems. *Biogeochemistry of Marine Dissolved Organic Matter* 137–246 (2024) doi:10.1016/B978-0-443-13858-4.00013-7.
2. Halsey, K. H. & Giovannoni, S. J. Biological controls on marine volatile organic compound emissions: A balancing act at the sea-air interface. *Earth Sci Rev* **240**, 104360 (2023).
3. Saha, M. & Fink, P. Algal volatiles – the overlooked chemical language of aquatic primary producers. *Biological Reviews* **97**, 2162–2173 (2022).
4. Shemi, A., Ben-Dor, S., Rotkopf, R., Dym, O. & Vardi, A. Phylogeny and biogeography of the algal DMS-releasing enzyme in the global ocean. *ISME Communications* **3**, (2023).
5. Xu, Q. *et al.* Volatile organic compounds released from *Microcystis flos-aquae* under nitrogen sources and their toxic effects on Chlorella vulgaris. *Ecotoxicol Environ Saf* **135**, 191–200 (2017).
6. Zuo, Z. J., Zhu, Y. R., Bai, Y. L. & Wang, Y. Volatile communication between *Chlamydomonas reinhardtii* cells under salt stress. *Biochem Syst Ecol* **40**, 19–24 (2012).
7. Dawson, R. A. *et al.* The microbiology of isoprene cycling in aquatic ecosystems. *Aquatic Microbial Ecology* **87**, 79–98 (2021).
8. Asher, E., Dacey, J. W., Ianson, D., Peña, A. & Tortell, P. D. Concentrations and cycling of DMS, DMSP, and DMSO in coastal and offshore waters of the Subarctic Pacific during summer, 2010-2011. *J Geophys Res Oceans* **122**, 3269–3286 (2017).

527 9. Pozzer, A. C., Gómez, P. A. & Weiss, J. Volatile organic compounds in aquatic
528 ecosystems – Detection, origin, significance and applications. *Science of the Total*
529 *Environment* **838**, (2022).

530 10. Moore, E. R., Weaver, A. J., Davis, E. W., Giovannoni, S. J. & Halsey, K. H. Metabolism
531 of key atmospheric volatile organic compounds by the marine heterotrophic bacterium
532 *Pelagibacter* HTCC1062 (SAR11). *Environ Microbiol* **24**, 212–222 (2022).

533 11. Rocco, M. *et al.* Oceanic phytoplankton are a potentially important source of benzenoids
534 to the remote marine atmosphere. *Communications Earth & Environment 2021 2:1* **2**, 1–8
535 (2021).

536 12. Misztal, P. K. *et al.* Atmospheric benzenoid emissions from plants rival those from fossil
537 fuels. *Scientific Reports 2015 5:1* **5**, 1–10 (2015).

538 13. Vila-Costa, M. *et al.* Phylogenetic identification and metabolism of marine
539 dimethylsulfide-consuming bacteria. *Environ Microbiol* **8**, 2189–2200 (2006).

540 14. Halsey, K. H., Padaki, V. G. & Giovannoni, S. The volatile organic carbon component of
541 dissolved organic matter in the ocean. *Biogeochemistry of Marine Dissolved Organic*
542 *Matter* 587–612 (2024) doi:10.1016/B978-0-443-13858-4.00001-0.

543 15. Moore, E. R., Davie-Martin, C. L., Giovannoni, S. J. & Halsey, K. H. *Pelagibacter*
544 metabolism of diatom-derived volatile organic compounds imposes an energetic tax on
545 photosynthetic carbon fixation. *Environ Microbiol* **22**, 1720–1733 (2020).

546 16. Wu, H. jun *et al.* Metagenomic analysis reveals specific BTEX degrading microorganisms
547 of a bacterial consortium. *AMB Express* **13**, (2023).

548 17. Bacosa, H. P., Mabuhay-Omar, J. A., Balisco, R. A. T., Omar, D. M. & Inoue, C.
549 Biodegradation of binary mixtures of octane with benzene, toluene, ethylbenzene or
550 xylene (BTEX): insights on the potential of *Burkholderia, Pseudomonas* and *Cupriavidus*
551 isolates. *World J Microbiol Biotechnol* **37**, 1–8 (2021).

552 18. Hocinat, A., Boudemagh, A., Ali-Khodja, H. & Medjemadj, M. Aerobic degradation of
553 BTEX compounds by *Streptomyces* species isolated from activated sludge and agricultural
554 soils. *Arch Microbiol* **202**, 2481–2492 (2020).

555 19. Khodaei, K., Nassery, H. R., Asadi, M. M., Mohammadzadeh, H. & Mahmoodlu, M. G.
556 BTEX biodegradation in contaminated groundwater using a novel strain (*Pseudomonas*
557 sp. BTEX-30). *Int Biodeterior Biodegradation* **116**, 234–242 (2017).

558 20. Jiang, B. *et al.* Biodegradation of Benzene, Toluene, Ethylbenzene, and o-, m-, and p-
559 Xylenes by the Newly Isolated Bacterium *Comamonas* sp. JB. *Appl Biochem Biotechnol*
560 **176**, 1700–1708 (2015).

561 21. Fu, H., Uchimiya, M., Gore, J. & Moran, M. A. Ecological drivers of bacterial community
562 assembly in synthetic phycospheres. *Proc Natl Acad Sci U S A* **117**, 3656–3662 (2020).

563 22. Seymour, J. R., Amin, S. A., Raina, J.-B. & Stocker, R. Zooming in on the phycosphere:
564 the ecological interface for phytoplankton–bacteria relationships. *Nat Microbiol* **2**, 17065
565 (2017).

566 23. Mitchell, J. G., Okubo, A. & Fuhrman, J. A. Microzones surrounding phytoplankton form
567 the basis for a stratified marine microbial ecosystem. *Nature 1985 316:6023* **316**, 58–59
568 (1985).

569 24. Seymour, J. R., Ahmed, T., Durham, W. M. & Stocker, R. Chemotactic response of
570 marine bacteria to the extracellular products of *Synechococcus* and *Prochlorococcus*.
571 *Aquatic Microbial Ecology* **59**, 161–168 (2010).

572 25. Smriga, S., Fernandez, V. I., Mitchell, J. G. & Stocker, R. Chemotaxis toward
573 phytoplankton drives organic matter partitioning among marine bacteria. *Proc Natl Acad*
574 *Sci U S A* **113**, 1576–1581 (2016).

575 26. Kogure, K., Simidu, U. & Taga, N. Bacterial attachment to phytoplankton in sea water. *J*
576 *Exp Mar Biol Ecol* **56**, 197–204 (1981).

577 27. Ramanan, R. *et al.* Phycosphere bacterial diversity in green algae reveals an apparent
578 similarity across habitats. *Algal Res* **8**, 140–144 (2015).

579 28. Raina, J. B. *et al.* Chemotaxis increases metabolic exchanges between marine
580 picophytoplankton and heterotrophic bacteria. *Nature Microbiology 2023 8:3* **8**, 510–521
581 (2023).

582 29. Ugolini, G. S. *et al.* Microfluidic approaches in microbial ecology. *Lab Chip* **24**, 1394–
583 1418 (2024).

584 30. Durham, B. P. *et al.* Cryptic carbon and sulfur cycling between surface ocean plankton.
585 *Proc Natl Acad Sci U S A* **112**, 453–457 (2015).

586 31. Nouchi, I., Hosono, T. & Sasaki, K. Seasonal changes in fluxes of methane and volatile
587 sulfur compounds from rice paddies and their concentrations in soil water. *Plant Soil* **195**,
588 233–245 (1997).

589 32. Brisson, V. *et al.* Identification of Effector Metabolites Using Exometabolite Profiling of
590 Diverse Microalgae. *mSystems* **6**, (2021).

591 33. Russo, A., Pollastri, S., Ruocco, M., Monti, M. M. & Loreto, F. Volatile organic
592 compounds in the interaction between plants and beneficial microorganisms. *J Plant*
593 *Interact* **17**, 840–852 (2022).

594 34. Yurimoto, H. & Sakai, Y. Interaction between C1-microorganisms and plants:
595 contribution to the global carbon cycle and microbial survival strategies in the
596 phyllosphere. *Biosci Biotechnol Biochem* **87**, 1–6 (2022).

597 35. Samo, T. J. *et al.* Attachment between heterotrophic bacteria and microalgae influences
598 symbiotic microscale interactions. *Environ Microbiol* **20**, 4385–4400 (2018).

36. Di Costanzo, F., Di Dato, V. & Romano, G. Diatom–Bacteria Interactions in the Marine Environment: Complexity, Heterogeneity, and Potential for Biotechnological Applications. *Microorganisms 2023, Vol. 11, Page 2967* **11**, 2967 (2023).

37. Wear, E. K., Carlson, C. A., Windecker, L. A. & Brzezinski, M. A. Roles of diatom nutrient stress and species identity in determining the short- and long-term bioavailability of diatom exudates to bacterioplankton. *Mar Chem* **177**, 335–348 (2015).

38. Liu, S. *et al.* Opportunities and challenges of using metagenomic data to bring uncultured microbes into cultivation. *Microbiome* **10**, (2022).

39. Wang, Y., Zhao, Y., Bollas, A., Wang, Y. & Au, K. F. Nanopore sequencing technology, bioinformatics and applications. *Nature Biotechnology 2021 39:11* **39**, 1348–1365 (2021).

40. Van Tol, H. M., Amin, S. A. & Virginia Armbrust, E. Ubiquitous marine bacterium inhibits diatom cell division. *ISME J* **11**, 31–42 (2017).

41. Helliwell, K. E., Shibl, A. A. & Amin, S. A. The Diatom Microbiome: New Perspectives for Diatom-Bacteria Symbioses. *The Molecular Life of Diatoms* 679–712 (2022) doi:10.1007/978-3-030-92499-7_23/COVER.

42. Balakrishnan, R., de Silva, R. T., Hwa, T. & Cremer, J. Suboptimal resource allocation in changing environments constrains response and growth in bacteria. *Mol Syst Biol* **17**, 10597 (2021).

43. Nelson, D. M., Tréguer, P., Brzezinski, M. A., Leynaert, A. & Quéguiner, B. Production and dissolution of biogenic silica in the ocean: Revised global estimates, comparison with regional data and relationship to biogenic sedimentation. *Global Biogeochem Cycles* **9**, 359–372 (1995).

44. Mayali, X. *et al.* Single-cell isotope tracing reveals functional guilds of bacteria associated with the diatom *Phaeodactylum tricornutum*. *Nat Commun* **14**, 5642 (2023).

45. Kim, H. *et al.* Bacterial response to spatial gradients of algal-derived nutrients in a porous microplate. *The ISME Journal 2021 16:4* **16**, 1036–1045 (2021).

46. Guillard, R. R. L. & Ryther, J. H. Studies of marine planktonic diatoms: *I. Cyclotella nana hustedt*, and *Detonula confervacea* (cleve) gran. *Can J Microbiol* **8**, 229–239 (1962).

47. Ritchie, R. J. Consistent Sets of Spectrophotometric Chlorophyll Equations for Acetone, Methanol and Ethanol Solvents. *Photosynth Res* **89**, 27–41 (2006).

48. Kolber, Z. S., Prášil, O. & Falkowski, P. G. Measurements of variable chlorophyll fluorescence using fast repetition rate techniques: defining methodology and experimental protocols. *Biochimica et Biophysica Acta (BBA) - Bioenergetics* **1367**, 88–106 (1998).

49. Halsey, K. H. *et al.* Biological cycling of volatile organic carbon by phytoplankton and bacterioplankton. *Limnol Oceanogr* **62**, 2650–2661 (2017).

50. Yáñez-Serrano, A. M. *et al.* GLOVOCS-Master compound assignment guide for proton transfer reaction mass spectrometry users. *Atmos Environ* **244**, 117929 (2021).

51. Holzinger, R. *et al.* Validity and limitations of simple reaction kinetics to calculate concentrations of organic compounds from ion counts in PTR-MS. *Atmos Meas Tech* **12**, 6193–6208 (2019).

52. Apweiler, R. *et al.* The Universal Protein Resource (UniProt) 2009. *Nucleic Acids Res.* **37**, D169–D174 (2008).

53. Pearson, W. R. An Introduction to Sequence Similarity ("Homology") Searching. *Current protocols in bioinformatics / editoral board, Andreas D. Baxevanis ... [et al.]* **0 3**, 10.1002/0471250953.bi0301s42 (2013).

54. Edgar, R. C. MUSCLE: multiple sequence alignment with high accuracy and high throughput. *Nucleic Acids Res* **32**, 1792 (2004).

55. Gu, Z. Complex heatmap visualization. *iMeta* **1**, (2022).

56. Gu, Z., Eils, R. & Schlesner, M. Complex heatmaps reveal patterns and correlations in multidimensional genomic data. *Bioinformatics* **32**, 2847–2849 (2016).

57. Lang, X. P., He, Z., Yang, G. P. & Dai, G. Physiological responses and altered halocarbon production in *Phaeodactylum tricornutum* after exposure to polystyrene microplastics. *Ecotoxicol Environ Saf* **268**, 115702 (2023).

58. Cabrita, M. T., Vale, C. & Rauter, A. P. Halogenated Compounds from Marine Algae. *Marine Drugs 2010, Vol. 8, Pages 2301-2317* **8**, 2301–2317 (2010).

59. Radman, S., Čagalj, M., Šimat, V. & Jerković, I. Seasonal Variability of Volatilome from *Dictyota dichotoma*. *Molecules 2022, Vol. 27, Page 3012* **27**, 3012 (2022).

60. Jerković, I. *et al.* Phytochemical study of the headspace volatile organic compounds of fresh algae and seagrass from the Adriatic Sea (single point collection). *PLoS One* **13**, (2018).

61. Koss, A. R. *et al.* Non-methane organic gas emissions from biomass burning: Identification, quantification, and emission factors from PTR-ToF during the FIREX 2016 laboratory experiment. *Atmos Chem Phys* **18**, 3299–3319 (2018).

62. Jakoncic, J., Jouanneau, Y., Meyer, C. & Stojanoff, V. The catalytic pocket of the ring-hydroxylating dioxygenase from *Sphingomonas* CHY-1. (2006) doi:10.1016/j.bbrc.2006.11.117.

63. Tan, H. M., Tang, H. Y., Joannou, C. L., Abdel-Wahab, N. H. & Mason, J. R. The *Pseudomonas putida* ML2 plasmid-encoded genes for benzene dioxygenase are unusual in codon usage and low in G + C content. *Gene* **130**, 33–39 (1993).

64. Bagnéris, C., Cammack, R. & Mason, J. R. Subtle Difference between Benzene and Toluene Dioxygenases of Pseudomonas putida. *Appl Environ Microbiol* **71**, 1570 (2005).

670 65. Kotani, T., Yurimoto, H., Kato, N. & Sakai, Y. Novel acetone metabolism in a propane-
671 utilizing bacterium, *Gordonia* sp. strain TY-5. *J Bacteriol* **189**, 886–893 (2007).

672 66. Chen, Y. C., Peoples, O. P. & Walsh, C. T. *Acinetobacter* cyclohexanone
673 monooxygenase: gene cloning and sequence determination. *J Bacteriol* **170**, 781 (1988).

674 67. Mangwani, N., Kumari, S. & Das, S. Involvement of quorum sensing genes in biofilm
675 development and degradation of polycyclic aromatic hydrocarbons by a marine bacterium
676 *Pseudomonas aeruginosa* N6P6. *Appl Microbiol Biotechnol* **99**, 10283–10297 (2015).

677 68. Olson, M. S., Ford, R. M., Smith, J. A. & Fernandez, E. J. Quantification of bacterial
678 chemotaxis in porous media using magnetic resonance imaging. *Environ Sci Technol* **38**,
679 3864–3870 (2004).

680 69. Lacal, J. *et al.* Bacterial chemotaxis towards aromatic hydrocarbons in *Pseudomonas*.
681 *Environ Microbiol* **13**, 1733–1744 (2011).

682 70. Matilla, M. A., Gavira, J. A. & Krell, T. Accessing nutrients as the primary benefit arising
683 from chemotaxis. *Curr Opin Microbiol* **75**, 102358 (2023).

684 71. Bell, W. & Mitchell, R. Chemotactic and growth responses of marine bacteria to algal
685 extracellular products. Biol. Bull. 143, 265–277 (1972).

686 72. Hearn, E. M., Patel, D. R. & Van Den Berg, B. Outer-membrane transport of aromatic
687 hydrocarbons as a first step in biodegradation. *Proc Natl Acad Sci U S A* **105**, 8601–8606
688 (2008).

689 73. Sun, J. *et al.* One Carbon Metabolism in SAR11 Pelagic Marine Bacteria. *PLoS One* **6**,
690 e23973 (2011).

691 74. Simó, R., Cortés-Greus, P., Rodríguez-Ros, P. & Masdeu-Navarro, M. Substantial loss of
692 isoprene in the surface ocean due to chemical and biological consumption.
693 *Communications Earth & Environment 2022 3:1* **3**, 1–8 (2022).

694 75. Davie-Martin, C. L., Giovannoni, S. J., Behrenfeld, M. J., Penta, W. B. & Halsey, K. H.
695 Seasonal and Spatial Variability in the Biogenic Production and Consumption of Volatile
696 Organic Compounds (VOCs) by Marine Plankton in the North Atlantic Ocean. *Front Mar*
697 *Sci* **7**, (2020).

698

699 **Figure Legends**:

700 **Fig. 1: VOC production in *P. tricornutum*. a** *m*/*z* signals (rows) produced during exponential
701 and stationary phases. The color scale ranges from low (light blue) to high (orange) production.
702 Black are *m*/*z* signals that were not detected in higher amounts in one of the phases than the
703 media control. Functional group categorization of each *m*/*z* signal is in the rightmost column. **b**

704 *P. tricornutum* growth (Error bars are SE for n=6 independent cultures). Arrows indicate
705 sampling days for VOCs.

706 **Fig. 2: Phycosphere bacteria demonstrate widely ranging VOC depletion patterns. a,b** *m/z*
707 depletion (rows) in each *P. tricornutum*–bacteria coculture (columns are labeled with the bacteria
708 grown with *P. tricornutum*) in exponential (**a**) and stationary phase (**b**) relative to axenic *P.*
709 *tricornutum* in each of the growth phases. The magnitude of depletion is shown, ranging from
710 low (light blue) to high (dark blue). Charcoal grey are *m/z* signals that were not depleted in
711 cocultures relative to the *P. tricornutum* monoculture. Pearson correlation distances were used to
712 cluster depletion patterns between PT-bacteria cocultures (top axes). Pie charts show the
713 proportion of each functional group depleted. **c** Growth of each bacteria (red lines) in coculture
714 with *P. tricornutum* (blue lines), (Error bars are SE, n=6). Arrows indicate sampling days for
715 VOCs. **d** Genes encoding hydrocarbon metabolism proteins in the phycosphere bacteria. Number
716 of gene copies is shown for each bacterium (bit-score $\geq$50, e-value >0.001). Abbreviations: *alkB*
717 (alkane-1-monooxygenase), *bnzA* (benzene dioxygenase alpha-subunit), *bnzB* (benzene
718 dioxygenase beta-subunit), *almA* (flavin-binding monooxygenase), *aor* (aldehyde
719 oxidoreductase), *acmA* (acetone monooxygenase).

720 **Fig. 3. Scanning electron microscopy images** showing (top panels) *Marinobacter* attached to
721 *P. tricornutum* in a flat orientation and (bottom panels) *Roseibium* attached to *P. tricornutum* in a
722 polar orientation.

723 **Fig. 4: Gross carbon production in *P. tricornutum* in the presence and absence of VOC**
724 **sinks (hydrocarbon trap or each bacteria in coculture).** Points are short-term (20 min) carbon
725 fixation rates, approximating gross carbon production (GCP) for each culture or coculture. Box
726 plots show the mean and upper and lower quartile divisions; red dots show data collected on day
727 4 (marked in Fig. 2c); blue dots & boxes show data collected on days (1, low box plot, and 5,
728 high box plot) in PT- *Roseibium*); whiskers show 95% confidence limits. Asterisks are GCP in
729 treatments (*P. tricornutum* with VOC trap and PT-cocultures) that were greater than GCP in
730 axenic *P. tricornutum* with no VOC trap for the same day in the growth curve (p-value < 0.05; t-
731 test). Inset shows the bacterial cell-normalized VOC depletion in each *P. tricornutum*-bacteria
732 coculture (Error bars are SE, n = 6).

733 **Fig. 5: Benzene incorporation into *Marinobacter* and *Rhodophyticola* biomass**. **a,c** Bacterial
734 cell densities in the presence (solid lines) and absence (dashed lines) of ^{13}C benzene in ASW
735 (blue, not done in *Rhodophyticola*), PTspent (olive), and coculture with *P. tricornutum* (orange).
736 Asterisks indicate treatments with higher cell densities in the presence of benzene compared to
737 the same media treatment with no added benzene ($p<0.05$, Error bars are SE, n = 3). **b,d** ^{13}C
738 enrichment in *Marinobacter* and *Rhodophyticola* in ASW (*Marinobacter* only), PTspent, and in
739 coculture with *P. tricornutum*. C_{net} is the fraction of biomass labeled from ^{13}C benzene. **e**
740 Bacterial C_{net} values in PT-*Marinobacter* and PT-*Rhodophyticola* with expanded y-axis. Insets
741 are SEM images of *Marinobacter* attached to *P. tricornutum* and *Rhodophyticola* unattached.

742

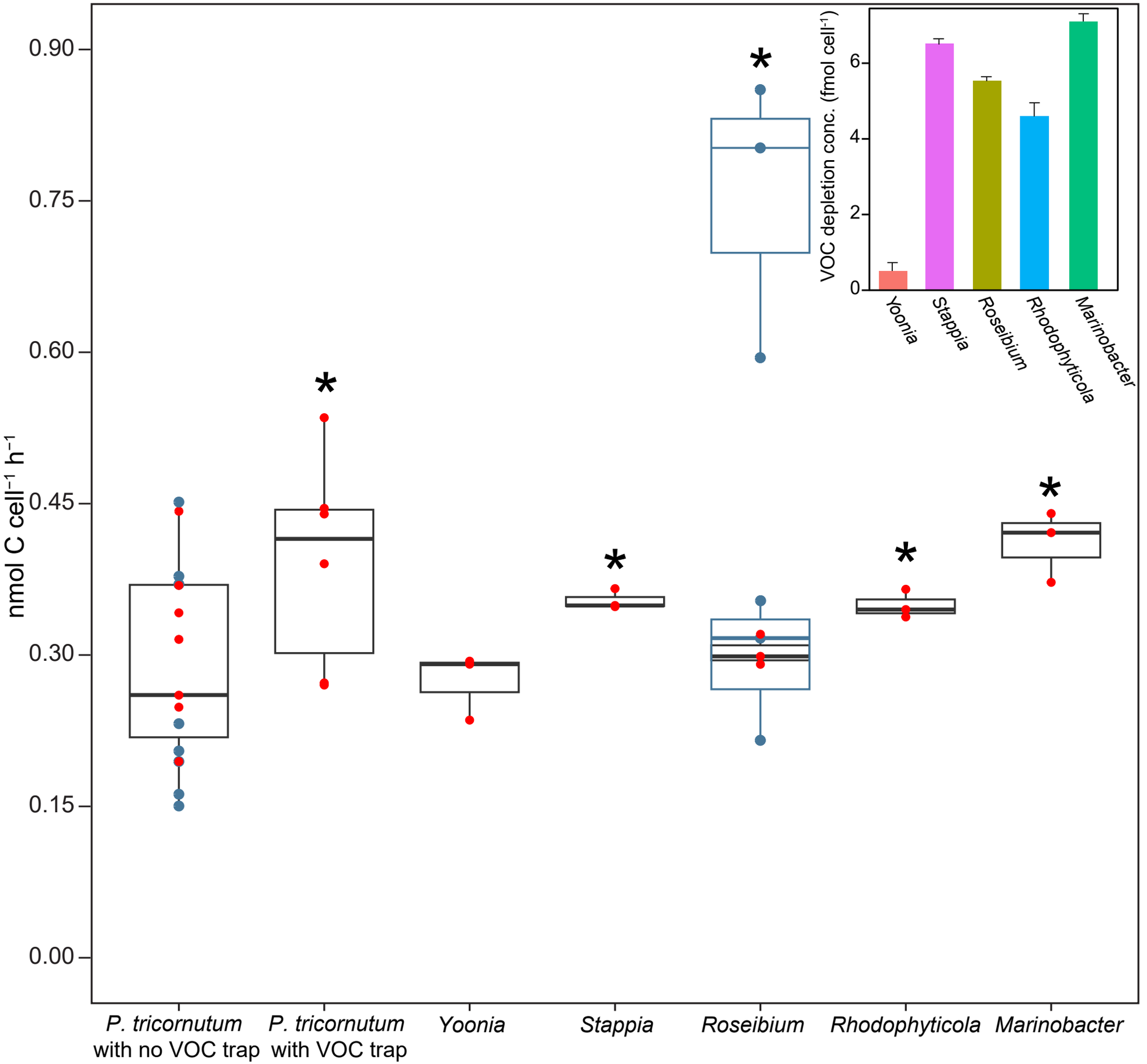
nmol C cell⁻¹ h⁻¹
0.90
0.75
0.60
0.45
0.30
0.15
0.00
*
*
*
*
*
P. tricornutum with no VOC trap
P. tricornutum with VOC trap
Yoonia
Stappia
Roseibium
Rhodophyticola
Marinobacter
VOC depletion conc. (fmol cell⁻¹)
0
2
4
6
Yoonia
Stappia
Roseibium
Rhodophyticola
Marinobacter

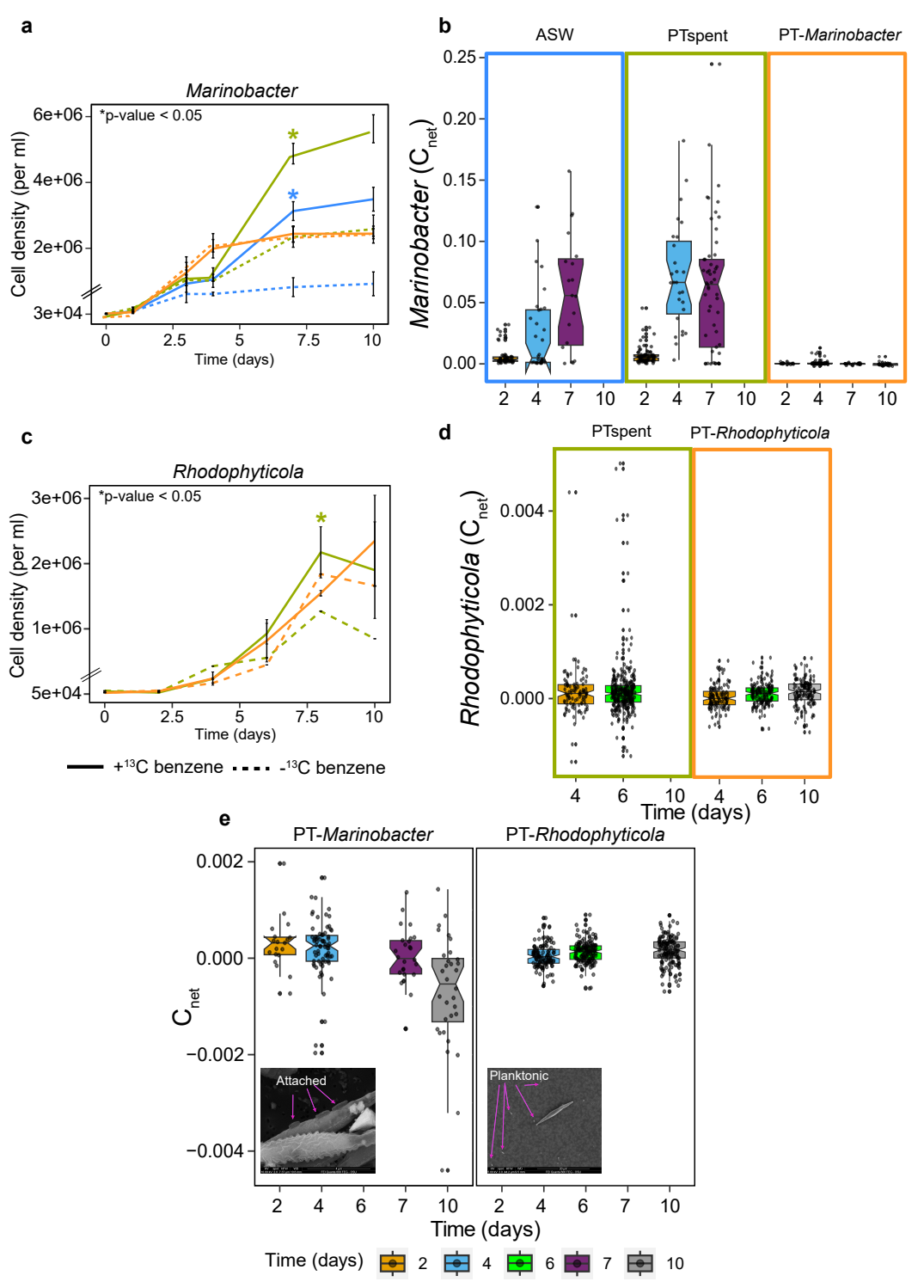
a
Marinobacter
*p-value < 0.05
Cell density (per ml)
6e+06
4e+06
2e+06
3e+04
0
2.5
5
7.5
10
Time (days)
b
ASW
PTspent
PT-Marinobacter
Marinobacter (Cnet)
0.25
0.20
0.15
0.10
0.05
0.00
2 4 7 10 2 4 7 10 2 4 7 10
c
Rhodophyticola
*p-value < 0.05
Cell density (per ml)
3e+06
2e+06
1e+06
5e+04
0
2.5
5
7.5
10
Time (days)
+13C benzene
-13C benzene
d
PTspent
PT-Rhodophyticola
Rhodophyticola (Cnet)
0.004
0.002
0.000
4 6 10 4 6 10
Time (days)
e
PT-Marinobacter
PT-Rhodophyticola
Cnet
0.002
0.000
−0.002
−0.004
Attached
Planktonic
2 4 6 7 10 2 4 6 7 10
Time (days)
Time (days)
2
4
6
7
10

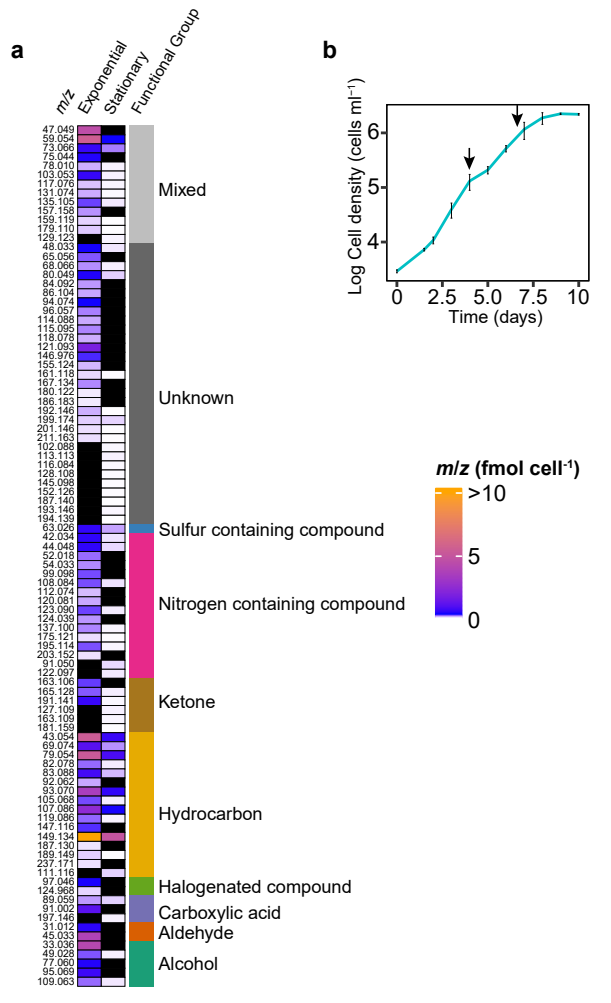
a
m/z
Exponential
Stationary
Functional Group
47.049
59.054
73.066
75.044
78.010
103.053
117.076
131.074
135.105
157.158
159.119
179.110
129.123
48.033
65.056
68.066
80.049
84.092
86.104
94.074
96.057
114.088
115.095
118.078
121.093
146.976
155.124
161.118
167.134
180.122
186.183
192.146
199.174
201.146
211.163
102.088
113.113
116.084
128.108
145.098
152.126
187.140
193.146
194.139
63.026
42.034
44.048
52.018
54.033
99.098
108.084
112.074
120.081
123.090
124.039
137.100
175.121
195.114
203.152
91.050
122.097
163.106
165.128
191.141
127.109
163.109
181.159
43.054
69.074
79.054
82.078
83.088
92.062
93.070
105.068
107.086
119.086
147.116
149.134
187.130
189.149
237.171
111.116
97.046
124.968
89.059
91.002
197.146
31.012
45.033
33.036
49.028
77.060
95.069
109.063
Mixed
Unknown
Sulfur containing compound
Nitrogen containing compound
Ketone
Hydrocarbon
Halogenated compound
Carboxylic acid
Aldehyde
Alcohol
b
Log Cell density (cells ml⁻¹)
6
5
4
0
2.5
5.0
7.5
10
Time (days)
m/z (fmol cell⁻¹)
>10
5
0

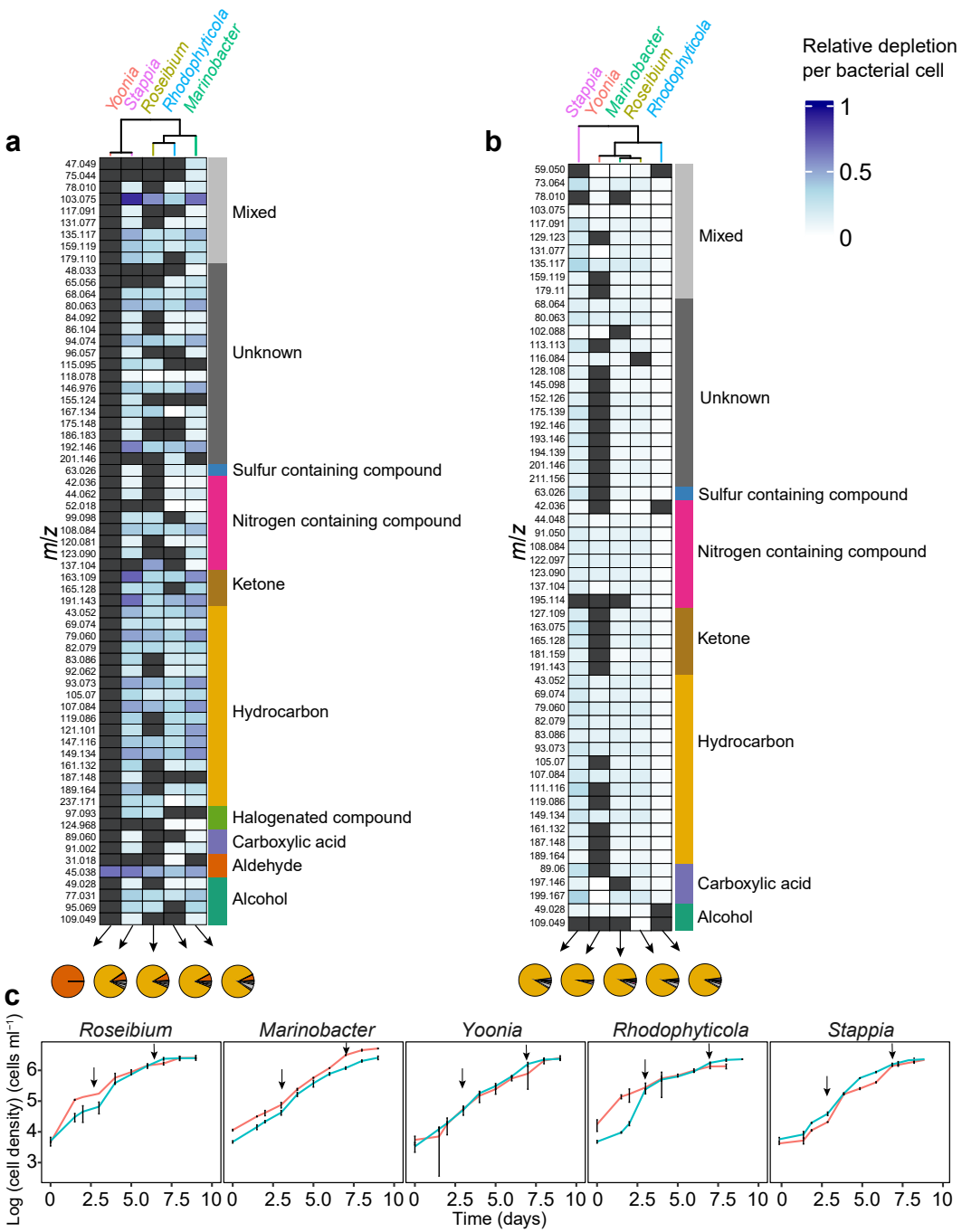

d

Bacterial species	*alkB*	*rhdA*	*bnzA*	*bnzB*	*almA*	*aor*	*acmA*
Marinobacter	2	1	1	1	2	1	2
Yoonia	0	0	0	0	0	2	0
Rhodophyticola	2	0	1	0	0	1	0
Roseibium	2	1	1	0	2	2	1
Stappia	0	0	0	0	1	1	1

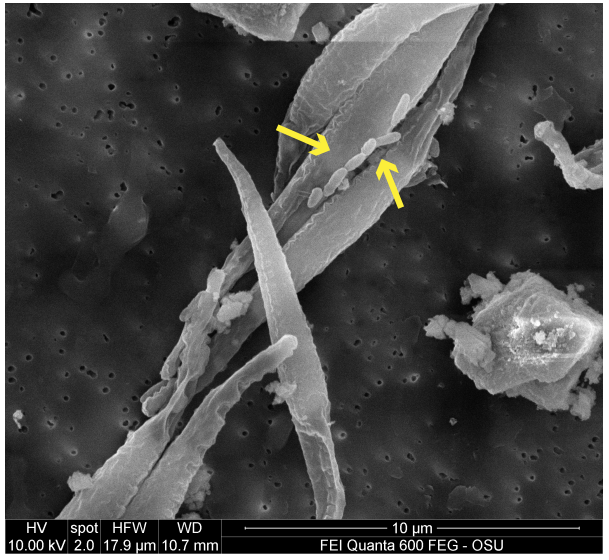
HV spot HFW WD
10.00 kV 2.0 17.9 µm 10.7 mm
10 µm
FEI Quanta 600 FEG - OSU

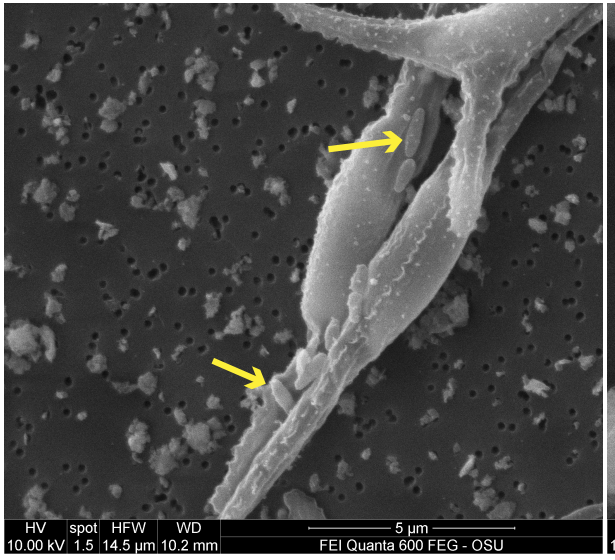
HV spot HFW WD
10.00 kV 1.5 14.5 µm 10.2 mm
5 µm
FEI Quanta 600 FEG - OSU

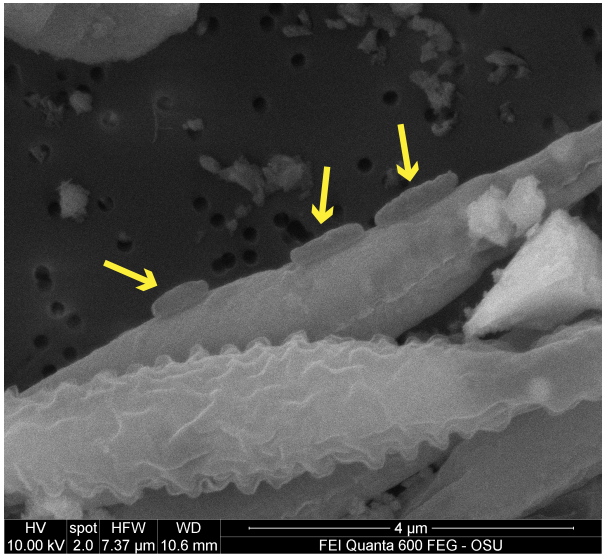
HV spot HFW WD
10.00 kV 2.0 7.37 µm 10.6 mm
4 µm
FEI Quanta 600 FEG - OSU

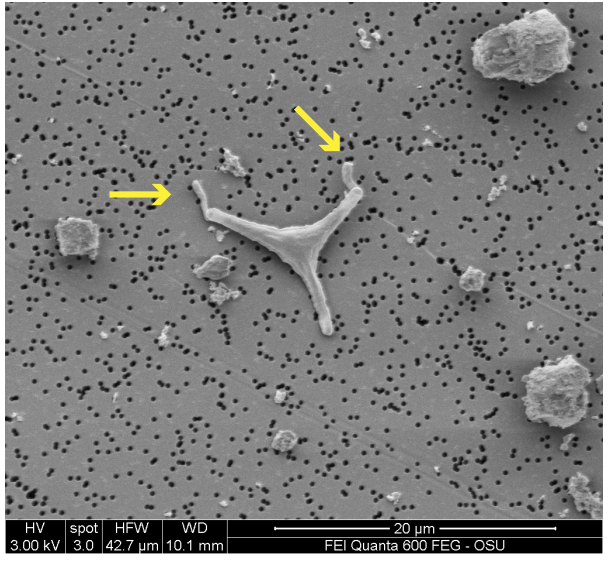
HV spot HFW WD
3.00 kV 3.0 42.7 µm 10.1 mm
20 µm
FEI Quanta 600 FEG - OSU

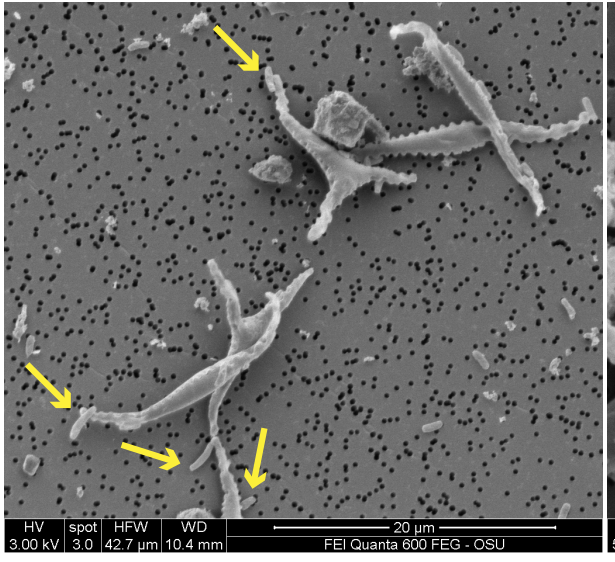
HV spot HFW WD
3.00 kV 3.0 42.7 µm 10.4 mm
20 µm
FEI Quanta 600 FEG - OSU

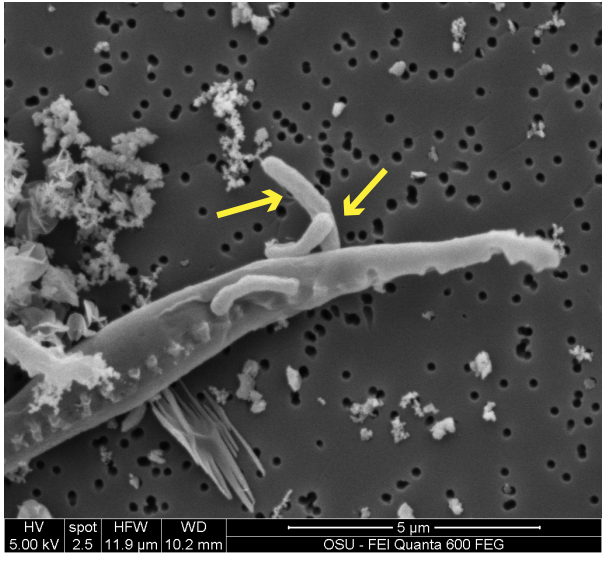
HV spot HFW WD
5.00 kV 2.5 11.9 µm 10.2 mm
5 µm
OSU - FEI Quanta 600 FEG